MIT Open Access Articles

Three-dimensional elastic constitutive relations of aligned carbon nanotube architectures

Massachusetts Institute of Technology

Three-Dimensional Elastic Constitutive Relations of Aligned Carbon Nanotube Architectures

Daniel Handlin,[1, a)] Itai Y. Stein,[2, a)] Roberto Guzman de Villoria,[1, b)] Hülya Cebeci,[1, c)] Ethan M. Parsons,[3] Simona Socrate,[3] Stephen Scotti,[4] and Brian L. Wardle[1, d)]

[1)] *Department of Aeronautics and Astronautics, Massachusetts Institute of Technology, 77 Massachusetts Ave, Cambridge, MA 02139, USA*

[2)] *Department of Mechanical Engineering, Massachusetts Institute of Technology, 77 Massachusetts Ave, Cambridge, MA 02139, USA*

[3)] *Institute for Soldier Nanotechnologies, Massachusetts Institute of Technology, 77 Massachusetts Ave, Cambridge, MA 02139, USA*

[4)] *NASA Langley Research Center, Hampton, VA 23681, USA*

Tailorable anisotropic intrinsic and scale-dependent properties of carbon nanotubes (CNTs) make them attractive elements in next-generation advanced materials. However, in order to model and predict the behavior of CNTs in macroscopic architectures, mechanical constitutive relations must be evaluated. This study presents the full stiffness tensor for aligned CNT-reinforced polymers as a function of the CNT packing (up to ~ 20 vol. %), revealing noticeable anisotropy. Finite element models reveal that the usually neglected CNT waviness dictates the degree of anisotropy and packing dependence of the mechanical behavior, rather than any of the usually cited aggregation or polymer interphase mechanisms. Combined with extensive morphology characterization, this work enables the evaluation of structure-property relations for such materials, enabling design of aligned CNT material architectures.

I. INTRODUCTION

Materials comprised of organized nanowires, nanofibers, and nanotubes can take advantage of intrinsic and scale dependent properties, such as phonon conduction, to create anisotropic tailored elements of next-generation architectures for a variety of high value applications, including sensors and actuators,[1–7] energy storage materials,[1,2,8–10] and transparent stretchable conductors.[1,2,8,11–17] To take full advantage of the anisotropic properties, a number of recent studies focused on the integration of aligned carbon nanotubes (CNTs) at a variety of CNT volume fractions (V_f) into a polymer matrix architecture,[18–22] forming an aligned CNT polymer nanocomposite (A-PNC). However, due to the limitations of sample size and testing techniques, which commonly include either bulk compression or nanoindentation,[18–20] previous studies were not able to determine the full constitutive relations for such materials.[18,20] Using uniaxial tensile tests, we quantify the mechanical behavior of high V_f (up to ~ 20 vol. %) aligned CNT (A-CNT) architectures along the longitudinal, transverse, and shear directions, and develop the first full set of elastic constitutive relations for an A-PNC material. The experimental results are then evaluated using previously reported finite element models,[20,23–26] which predict the effect of CNT waviness on the elastic modulus of the A-PNC, showing that CNT

waviness has a very large impact on the A-PNC stiffness. These findings enable the establishment of better structure-property relations for A-CNT materials, which could allow the design and fabrication of A-PNCs with enhanced performance, such as actuation efficiency,[5] transport properties,[5,21,22] and elastic anisotropy.[5,20]

CNT reinforcement of macroscopic structures stems from their unrivaled theoretical mechanical and transport properties, as well as scale-dependent effects that include thermal boundary resistance and the pullout toughness associated with a high aspect ratio.[14,27] A number of recent studies reported the fabrication of novel materials with exciting properties via the addition of CNT fillers, which form an unaligned percolated CNT network.[13–15,27] However, the fabrication of such materials was limited to low V_f ($\lesssim 1$ vol. % CNTs) since enhancement of the material properties is conditional on optimal CNT dispersion,[28] which is unattainable at high CNT volume fractions without damaging chemical processing, such as functionalization.[14] A fabrication method that could alleviate the problems associated with CNT phase separation is wet infusion, where a liquid phase polymer is introduced into a pre-existing network of CNTs. One example would be the fabrication of nanocomposites using the previously reported CNT aerogel architecture,[16,29–31] but due to the small pore sizes in CNT aerogels,[29] the infusion of matrix materials into such architectures usually requires a pressure differential that may damage the very fragile CNT network. Another problem of polymer nanocomposites formed using unaligned CNTs is that a uniform dispersion of CNTs leads to isotropic nanocomposite properties, which cannot be optimized for any single operating direction. These two shortcomings can be remedied by using aligned networks of CNTs, known as forests, where capillary forces can be used to aid with the polymer infusion,[19,32–34] and where

---

a) These authors contributed equally to this work

b) Current address: IMDEA Materials Institute, C/Eric Kandel 2, 28906 Getafe, Madrid, Spain

c) Current address: Department of Aeronautical Engineering, Istanbul Technical University, Maslak 34469, Istanbul, Turkey

d) Electronic mail: wardle@mit.edu

A-PNCs with anisotropic properties can be formed. Here the anisotropy in stiffness of variable V_f A-PNCs formed via capillary-induced wetting is quantified, and their full three dimensional elastic constitutive relations are developed.

II. METHODS

Here we describe the methodology used to investigate the mechanical behavior of A-PNCs comprised of $\sim 1-20$ vol. %, ~ 8 nm outer diameter, A-CNTs.

A. A-PNC Fabrication, Processing, and Morphology Characterization

A-CNT forests were grown in a 22 mm internal diameter quartz tube furnace at atmospheric pressure via a previously described thermal catalytic chemical vapor deposition process using ethylene as the carbon source.[19,21,22] The forests were grown on 1 cm $\times$ 1 cm Si substrates with a catalytic layer composed of 1 nm Fe/10 nm Al_2O_3 deposited via electron beam physical vapor deposition. Previous studies on the as-grown multiwalled CNTs determined that the CNTs in the forest have an average outer diameter of ~ 8 nm,[35] inter-CNT spacing of ~ 80 nm,[36] and V_f of ~ 1 vol. % CNTs.[35] The CNT forests are then delaminated from the Si substrate using a standard lab razor blade, and mechanically densified (biaxially) to the desired V_f (up to ~ 20 vol. % CNTs),[27,36] forming continuous and spatially homogeneous A-CNT architectures.[19,22,36]

To form the A-PNCs, degassed aerospace-grade epoxy (Hexcel RTM6), heated to 90°C, was first placed in the center of a teflon mold. The CNT forest was then placed on top of the epoxy, which then slowly infused the forest due to capillary forces. The wetted CNT forest was subsequently cured at 160°C for 75 minutes. The cured A-PNC block was then placed into a silicone dogbone mold in the desired tensile testing orientation: CNT alignment parallel to the dogbone axis for E_x and ν_{xy}; perpendicular to the dogbone axis for E_y and ν_{yz}; and at 45° to the dogbone axis for G_{xy}. The remainder of the mold was then filled with epoxy and cured at 180°C for 120 minutes.

The surface morphology of the A-CNTs and A-PNCs was characterized using a JEOL 6700 cold field-emission gun high resolution scanning electron microscope (HRSEM) using secondary electron imaging at a working distance of 3.0 mm and the following accelerating voltages: 1.0 for A-CNTs with V_f up to 5% CNTs, 1.5 kV for A-CNTs with $V_f > 5\%$ CNTs, and 3.0 kV for A-PNCs. See Fig. 1 for HRSEM images of the cross-sections of an as-grown ($V_f \sim 1\%$) and densified ($V_f \sim 18\%$) A-CNT forests, and an A-PNC with $V_f \sim 18\%$ CNTs.

In preparation for the optical strain mapping, also known as digital image correlation (DIC), samples were
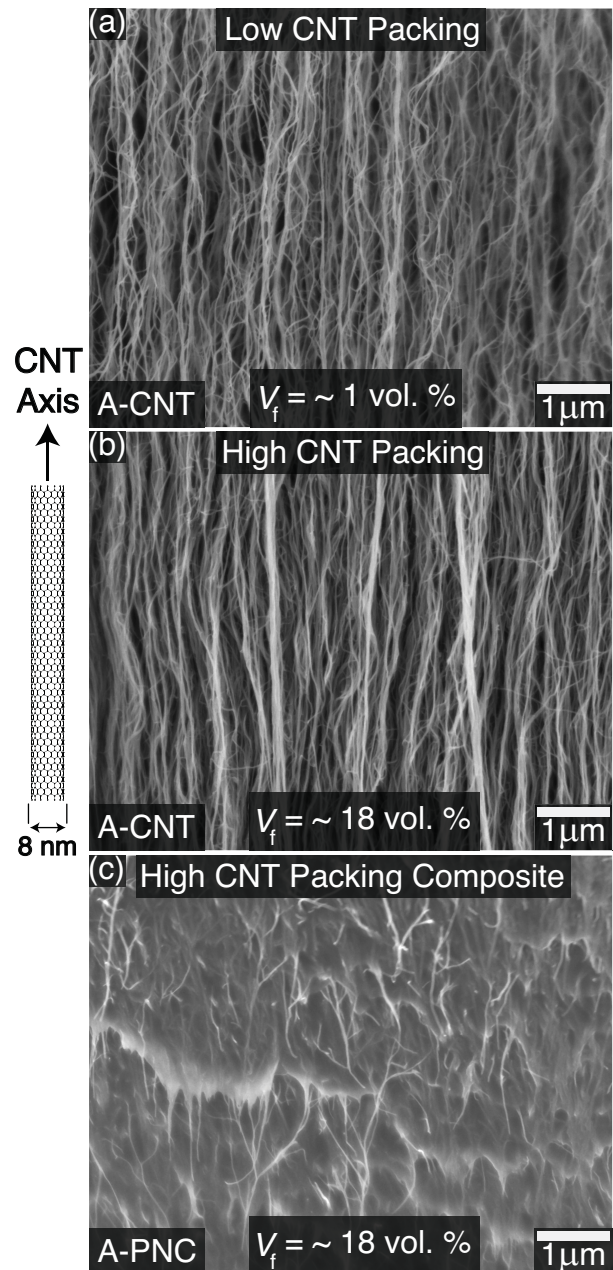

FIG. 1. HRSEM images of the cross-sectional morphology of as-grown ~ 1 vol. % aligned carbon nanotubes, A-CNTs (a), densified ~ 18 vol. % A-CNTs (b) and ~ 18 vol. % A-CNT polymer nanocomposites, A-PNCs (c).

polished, spray painted white, and speckled black. Additional details can be found elsewhere.[37]

B. Mechanical Testing

To establish the anisotropic elastic constitutive relations of the A-PNCs, elements of the stiffness tensor, c_{ijkl}, are determined via typical engineering quantities that include the A-PNC moduli, both elastic (E) and

shear (G), and Poisson ratios (ν). These quantities are evaluated via uniaxial tensile testing using a Zwick Z-010 tensile testing machine with a 500 N load cell, and are evaluated along three material directions: longitudinal (yielding E_x and ν_{xy}); transverse (yielding E_y and ν_{yz}); and shear (yielding G_{xy}). See Fig. 2a for an illustration of the three tensile testing geometries, where the CNT primary axis is in the x direction. To map the evolution of strain in the tensile tests with a high degree of accuracy, DIC was performed using the Vic 2D software from Correlated Solutions, Inc. This method is well known for its high resolution,[37] and was recently used to determine the moduli (elastic and shear),[38] and Poisson ratios,[38,39] of low V_f ($\simeq 1$ vol. % CNTs) polymer composites. See Fig. 2b for a sample strain field evaluated using DIC showing that the A-PNC undergoes less deformation than the pure polymer during testing, and Fig. 2c for a stress (σ) vs. strain (ε) plot showing that the A-PNCs have a higher elastic modulus ($E \sim 3.9$ GPa and ~ 6.2 GPa) than the pure polymer ($E \sim 2.9$ GPa). Using this methodology, the mechanical behavior of A-PNCs with V_f up to ~ 20 vol. % CNTs is studied, corresponding to inter-CNT distances of ~ 10 nm for average packing that is between square and hexagonal.[36]

C.   Evaluation of the Elastic Stiffness Tensor

Once the A-PNC moduli and Poisson ratios are known, the full compliance tensor (s_{ijkl}) can be evaluated from the generalized Hooke's law for transversely isotropic materials:[40]

$$\varepsilon_{ij} = s_{ijkl}\sigma_{kl} \tag{1a}$$

$$s_{ijkl} = \begin{bmatrix} \frac{1}{E_x} & \frac{-\nu_{xy}}{E_x} & \frac{-\nu_{xy}}{E_x} & 0 & 0 & 0 \\ \frac{-\nu_{xy}}{E_x} & \frac{1}{E_y} & \frac{-\nu_{yz}}{E_y} & 0 & 0 & 0 \\ \frac{-\nu_{xy}}{E_x} & \frac{-\nu_{yz}}{E_y} & \frac{1}{E_y} & 0 & 0 & 0 \\ 0 & 0 & 0 & \frac{1+\nu_{yz}}{E_y} & 0 & 0 \\ 0 & 0 & 0 & 0 & \frac{1}{2G_{xy}} & 0 \\ 0 & 0 & 0 & 0 & 0 & \frac{1}{2G_{xy}} \end{bmatrix} \tag{1b}$$

By rearranging Eq. 1a, the elasticity tensor (c_{ijkl}) can now be evaluated ($x \equiv 1$, $y \equiv 2$, $z \equiv 3$):

$$\sigma_{ij} = c_{ijkl}\varepsilon_{kl} = s_{ijkl}^{-1}\varepsilon_{kl} \tag{2a}$$

$$c_{ijkl} = \begin{bmatrix} c_{1111} & c_{1122} & c_{1122} & 0 & 0 & 0 \\ c_{1122} & c_{2222} & c_{2233} & 0 & 0 & 0 \\ c_{1122} & c_{2233} & c_{2222} & 0 & 0 & 0 \\ 0 & 0 & 0 & 2c_{2323} & 0 & 0 \\ 0 & 0 & 0 & 0 & 2c_{1212} & 0 \\ 0 & 0 & 0 & 0 & 0 & 2c_{1212} \end{bmatrix} \tag{2b}$$

See Table I for the resulting values of the elements of c_{ijkl} for A-PNCs as a function of V_f (up to $\sim 18\%$).
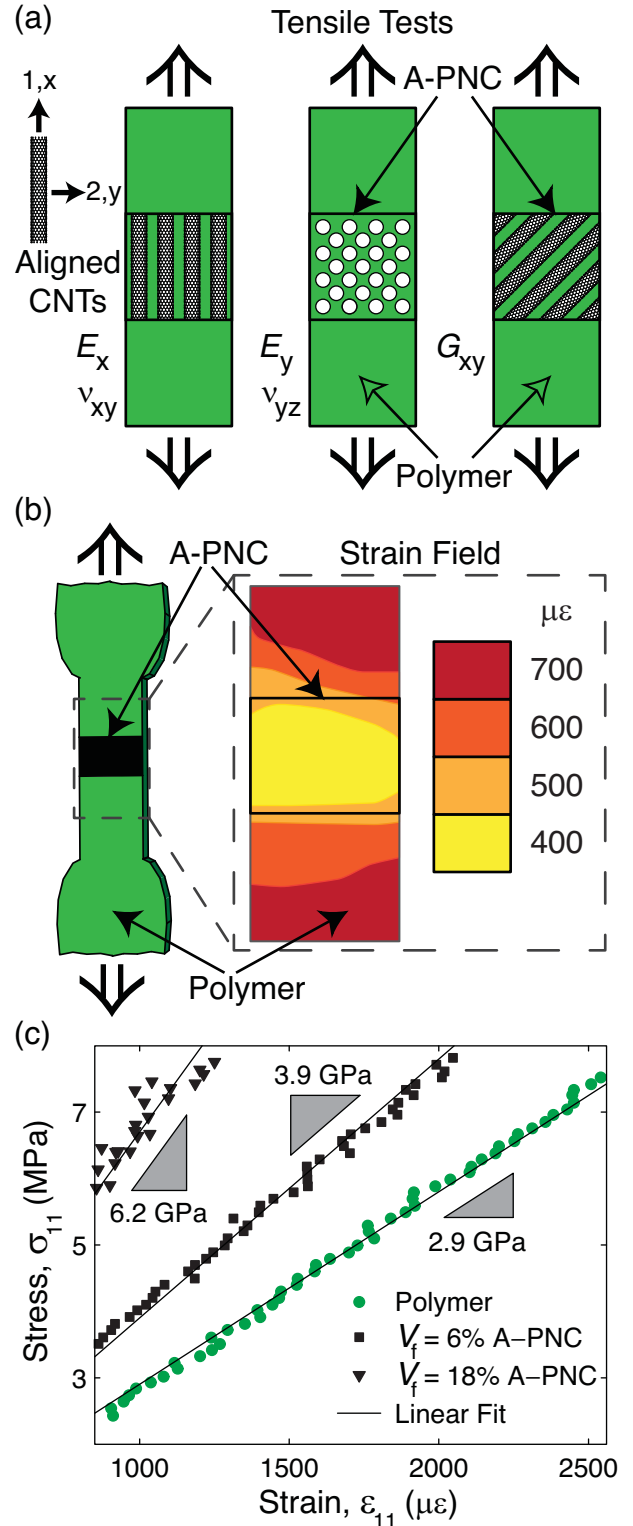

FIG. 2. Illustration of the Tensile testing geometry (a), a sample of how digital image correlation (DIC) was used to experimentally determine the elastic modulus (b), and a sample stress-strain curve showing that the A-PNCs have a higher modulus than the baseline unreinforced polymer (c).
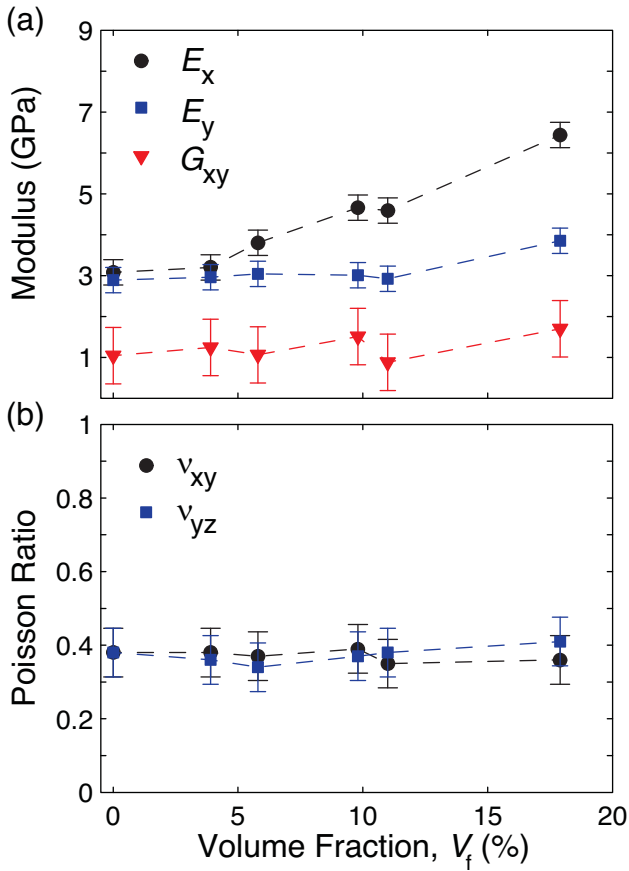
FIG. 3. Plot of the elastic, E, and shear, G, moduli (a), and Poisson ratios, ν (b), for A-PNCs at a variety of CNT volume fractions, V_f. See Fig. 2 for illustration of their experimental determination.

III. RESULTS AND DISCUSSION

The effect of CNT packing (V_f) on the A-PNC constitutive elements was determined from the tensile test derived stress-strain curves, as summarized in Fig. 3 for the moduli (Fig. 3a) and Poisson ratios (Fig. 3b). While E_y and G_{xy} are either unchanged or see small enhancements as V_f increases ($E_y \sim 3$ GPa and $G_{xy} \sim 1$ GPa), E_x sees a linear increase as V_f increases, more than doubling (from ~ 3.1 GPa for the baseline to ~ 6.4 GPa) for A-PNCs made using 18 vol. % CNT forests. This enhancement in E_x is similar to the one observed in a previous nanoindentation study,[20,26] however the A-PNC modulus at $V_f = 18$ vol. % CNTs is still far from the one predicted by a simple rule of mixtures analysis for collimated CNTs in a matrix, which predicts E_x to be ~ 60 GPa for $V_f = 18\%$ (assuming intrinsic CNT modulus $\simeq 500$ GPa), rather than the ~ 6 GPa we measured. This order of magnitude difference in expectation vs. measured CNT reinforcement is typically attributed to inadequate bonding of the CNTs to the polymer matrix, or phase separation/homogeneity issues, and/or the formation of an interphase region. None of these explanations
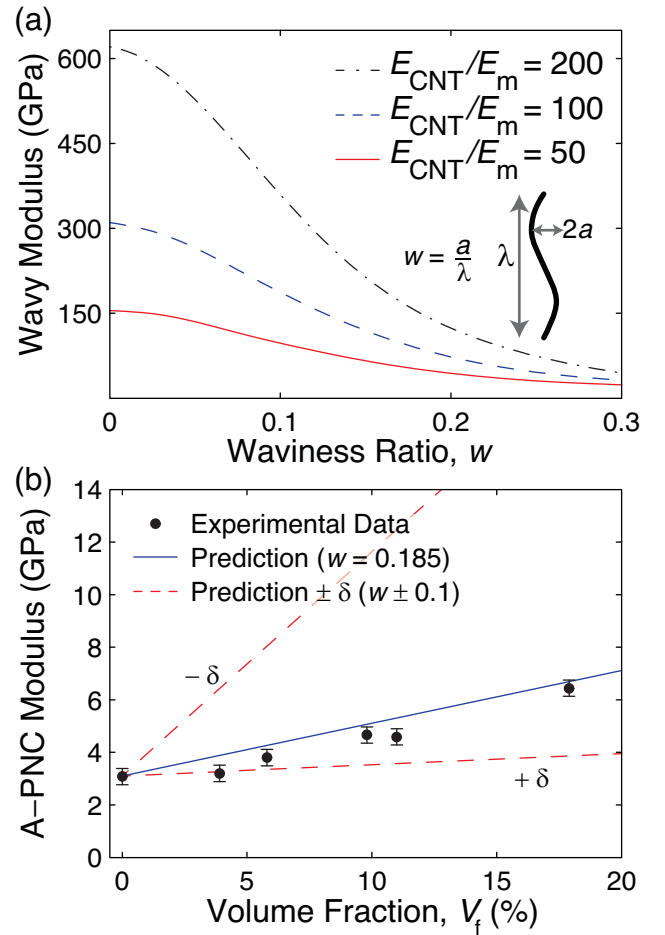

FIG. 4. Plot of the wavy CNT modulus as a function of the CNT waviness ratio, w (a), and prediction of the A-PNC longitudinal modulus as a function of the CNT volume fraction, V_f.[26] The wavy modulus was calculated for ratios of the intrinsic modulus of a collimated CNT, E_{CNT}, and the modulus of the polymer matrix, E_m, ranging from 50 to 200 using a previously reported finite element model.[23]

is viable for the system studied here due to the method of sample preparation and lack of any observable interphase in the epoxy A-PNC samples.[19] However, previously reported finite element models have demonstrated that the waviness of the CNTs can strongly influence the A-PNCs modulus, and could lead to composite moduli that are more than an order of magnitude lower than the ones predicted by rule of mixtures analysis of collimated CNTs.[20,23–26]

To model the effective reinforcing modulus of a wavy CNT in the polymer matrix (wavy modulus) as a function of CNT waviness, three primary quantities need to be evaluated: intrinsic modulus of a collimated CNT (E_{CNT}); modulus of the polymer matrix (E_m), which is ~ 3.1 GPa for our epoxy (see Fig. 3a); and the waviness ratio for CNTs with a sinusoidal shape (w).[23] See Fig. 4a for a plot of wavy modulus vs. w for E_{CNT}/E_m ranging from 50 to 200, determined using a previously

TABLE I. Elements of the elasticity tensor (c_{ijkl}) as a function of CNT volume fraction (V_f). c_{2323}, while not independent, is provided for completeness.

V_f	c_{1111} (GPa)	c_{2222} (GPa)	c_{1122} (GPa)	c_{2233} (GPa)	c_{2323} (GPa)	c_{1212} (GPa)
0	5.47	5.19	3.15	3.09	0.52	0.52
3.9	5.49	5.06	3.02	2.88	0.54	0.62
5.8	5.69	4.58	2.55	2.31	0.57	0.53
9.8	6.77	4.57	2.71	2.37	0.55	0.76
11.0	6.13	4.20	2.20	2.09	0.53	0.44
17.9	8.73	5.79	3.19	3.06	0.68	0.85

reported finite element model.[23] Using $E_{CNT} \sim 500$ GPa ($\Rightarrow E_{CNT}/E_m \sim 160$),[20,23,26] and $w = 0.185 \pm 0.1$,[20,26] an E_x of ~ 6.7 GPa at $w = 0.185$ and $V_f = 18$ vol. % CNTs is predicted (see Fig. 4b).[26] Also, as illustrated by Fig. 4b, the waviness of the CNTs in the A-PNCs appears to decrease significantly as V_f is increased, from $w \sim 0.285$ at $V_f = 4$ vol. % CNTs ($\sim 2\%$ overprediction) to $w \sim 0.185$ at $V_f = 18$ vol. % CNTs ($\sim 4\%$ overprediction). This is likely due to CNT crowding during the densification process, and strongly agrees with the observations of a recent morphological study on CNT forests of varying V_f.[36] When coupled with more accurate models for CNT waviness,[36] and the ability to use non-constant waviness ratios when modeling elastic moduli, accurate predictions of the mechanical behavior of A-PNCs at a variety of CNT V_f are enabled. Accuracy in such models is critical for many applications, e.g. hierarchical composites, where modeling relies on such constitutive relations for prediction of load-transfer properties.[41]

As presented in Fig. 3b, ν_{xy} and ν_{yz} are largely unaffected by the increase in V_f (ν_{xy} and $\nu_{yz} \simeq 0.37$), but may vary by more than 10% from sample to sample. This is important because most studies usually assume that the Poisson ratios are isotropic and constant (~ 0.3),[20,23–26] but Fig. 3b shows that these assumptions may not be adequate for accurate modeling of the A-PNC system. The elastic stiffness tensor, c_{ijkl}, is evaluated for all V_f and can be found in Table I.

IV. CONCLUSION

In summary, the full elastic constitutive relations, c_{ijkl}, for A-PNCs of varying CNT volume fractions were reported for the first time. The experimental results show that while the transverse and shear moduli see little to no change as V_f increases, the longitudinal modulus is continually enhanced as V_f increases (up to $\sim 20\%$), and exhibits an increase of more than 100% at $V_f = 18$ vol. % CNTs. Because a simple rule of mixtures analysis for collimated CNTs in a polymer matrix overpredicts the A-PNC longitudinal modulus by more than an order of magnitude, previously reported finite element models for wavy CNTs were applied to the A-PNCs, and yielded predictions for the longitudinal modulus that were within 5% of the experimentally determined values. Future work should explore the use of non-constant CNT waviness ratios, the development of a model to better quantify the CNT waviness, and the extension of the finite element models to allow the prediction of both transverse and shear moduli. Using the constitutive relations reported here, A-PNCs with optimized properties can be designed for next-generation sensors and actuators, energy storage materials, transparent stretchable conductors, and hierarchical composites.

[1] M. F. L. De Volder, S. H. Tawfick, R. H. Baughman, and A. J. Hart, Science 339, 535 (2013).
[2] T.-W. Chou, L. Gao, E. T. Thostenson, Z. Zhang, and J.-H. Byun, Compos. Sci. Technol. 70, 1 (2010).
[3] C. Li, E. T. Thostenson, and T.-W. Chou, Compos. Sci. Technol. 68, 1227 (2008).
[4] K. Mukai, K. Asaka, T. Sugino, K. Kiyohara, I. Takeuchi, N. Terasawa, D. N. Futaba, K. Hata, T. Fukushima, and T. Aida, Adv. Mater. 21, 1582 (2009).

[5] S. Liu, Y. Liu, H. Cebeci, R. Guzman de Villoria, J.-H. Lin, B. L. Wardle, and Q. M. Zhang, Adv. Funct. Mater. **20**, 3266 (2010).

[6] L. Lu and W. Chen, Adv. Mater. **22**, 3745 (2010).

[7] L. Lu, J. Liu, Y. Hu, Y. Zhang, H. Randriamahazaka, and W. Chen, Adv. Mater. **24**, 4317 (2012).

[8] M. N. Hyder, S. W. Lee, F. c. Cebeci, D. J. Schmidt, Y. Shao-Horn, and P. T. Hammond, ACS Nano **5**, 8552 (2011).

[9] X. Wang, X. Han, M. Lim, N. Singh, C. L. Gan, M. Jan, and P. S. Lee, J. Phys. Chem. C **116**, 12448 (2012).

[10] R. Van Noorden, Nature **469**, 14 (2011).

[11] T. Sekitani, Y. Noguchi, K. Hata, T. Fukushima, T. Aida, and T. Someya, Science **321**, 1468 (2008).

[12] T. Sekitani, H. Nakajima, H. Maeda, T. Fukushima, T. Aida, K. Hata, and T. Someya, Nat. Mater. **8**, 494 (2009).

[13] K.-Y. Chun, Y. Oh, J. Rho, J.-H. Ahn, Y.-J. Kim, H. R. Choi, and S. Baik, Nat. Nanotechnol. **5**, 853 (2010).

[14] D. S. Hecht, L. Hu, and G. Irvin, Adv. Mater. **23**, 1482 (2011).

[15] D. J. Lipomi, M. Vosgueritchian, B. C.-K. Tee, S. L. Hellstrom, J. A. Lee, C. H. Fox, and Z. Bao, Nat. Nanotechnol. **6**, 788 (2011).

[16] K. H. Kim, M. Vural, and M. F. Islam, Adv. Mater. **23**, 2865 (2011).

[17] F. Mirri, A. W. K. Ma, T. T. Hsu, N. Behabtu, S. L. Eichmann, C. C. Young, D. E. Tsentalovich, and M. Pasquali, ACS Nano **6**, 9737 (2012).

[18] E. García, A. Hart, B. Wardle, and A. Slocum, Adv. Mater. **19**, 2151 (2007).

[19] B. L. Wardle, D. S. Saito, E. J. García, A. J. Hart, R. Guzman de Villoria, and E. A. Verploegen, Adv. Mater. **20**, 2707 (2008).

[20] H. Cebeci, R. Guzman de Villoria, A. J. Hart, and B. L. Wardle, Compos. Sci. Technol. **69**, 2649 (2009).

[21] S. Vaddiraju, H. Cebeci, K. K. Gleason, and B. L. Wardle, ACS Appl. Mater. Interfaces **1**, 2565 (2009).

[22] A. M. Marconnet, N. Yamamoto, M. A. Panzer, B. L. Wardle, and K. E. Goodson, ACS Nano **5**, 4818 (2011).

[23] F. T. Fisher, R. D. Bradshaw, and L. C. Brinson, Appl. Phys. Lett. **80**, 4647 (2002).

[24] F. Fisher, R. Bradshaw, and L. Brinson, *Modeling and Characterization of Nanostructured Materials*, Compos. Sci. Technol. **63**, 1689 (2003).

[25] R. Bradshaw, F. Fisher, and L. Brinson, *Modeling and Characterization of Nanostructured Materials*, Compos. Sci. Technol. **63**, 1705 (2003).

[26] H. Cebeci, *Multifunctional Properties of Controlled Morphology Aligned Carbon Nanotube Polymer Nanocomposites and Their Applications*, Ph.D. thesis, Istanbul Technical University (2011).

[27] L. Liu, W. Ma, and Z. Zhang, Small **7**, 1504 (2011).

[28] Y. Y. Huang and E. M. Terentjev, Adv. Funct. Mater. **20**, 4062 (2010).

[29] M. Bryning, D. Milkie, M. Islam, L. Hough, J. Kikkawa, and A. Yodh, Adv. Mater. **19**, 661 (2007).

[30] J. Zou, J. Liu, A. S. Karakoti, A. Kumar, D. Joung, Q. Li, S. I. Khondaker, S. Seal, and L. Zhai, ACS Nano **4**, 7293 (2010).

[31] K. H. Kim, Y. Oh, and M. F. Islam, Nat. Nanotechnol. **7**, 562 (2012).

[32] H. Liu, J. Zhai, and L. Jiang, Soft Matter **2**, 811 (2006).

[33] X. Huang, J. J. Zhou, E. Sansom, M. Gharib, and S. C. Haur, Nanotechnology **18**, 305301 (2007).

[34] M. K. Shin, J. Oh, M. Lima, M. E. Kozlov, S. J. Kim, and R. H. Baughman, Adv. Mater. **22**, 2663 (2010).

[35] A. J. Hart and A. H. Slocum, J. Phys. Chem. B **110**, 8250 (2006).

[36] I. Y. Stein and B. L. Wardle, Phys. Chem. Chem. Phys. **15**, 4033 (2013).

[37] D. A. Handlin, *Three-Dimensional Constitutive Relations of Aligned Carbon Nanotube Polymer Nanocomposites*, Master's thesis, Massachusetts Institute of Technology (2013).

[38] A. T. Sepúlveda, R. Guzman de Villoria, J. C. Viana, A. J. Pontes, B. L. Wardle, and L. A. Rocha, Nanoscale **5**, 4847 (2013).

[39] R. H. Pritchard, P. Lava, D. Debruyne, and E. M. Terentjev, Soft Matter **9**, 6037 (2013).

[40] D. Allen and W. Haisler, *Introduction to Aerospace Structural Analysis* (Wiley, 1985).

[41] S. I. Kundalwal and M. C. Ray, J. Appl. Mech. **80**, 021010 (2013).